Thermal Conductivity of Carbon Nanotube Array Laminated Composite Materials

Jandro L. Abot, Gregory Bardin, Courtney Spriegel, Yi Song, Vasudevan Raghavan and Nirmal Govindaraju

Journal of Composite Materials 2011 45: 321 originally published online 9 September 2010
DOI: 10.1177/0021998310373512

Thermal Conductivity of Carbon Nanotube Array Laminated Composite Materials

JANDRO L. ABOT,* GREGORY BARDIN, COURTNEY SPRIEGEL AND YI SONG
Department of Aerospace Engineering and Engineering Mechanics
University of Cincinnati, Cincinnati, OH 45221-0070, USA

VASUDEVAN RAGHAVAN
Department of Mechanical Engineering, University of Cincinnati
Cincinnati, OH 45221-0072, USA

NIRMAL GOVINDARAJU
Department of Chemical and Materials Engineering, University of Cincinnati
Cincinnati, OH 45221-0012, USA

ABSTRACT: Thermal transport of laminated composite materials in their through-the-thickness direction is known to be significantly lower than in the in-plane laminate directions. This article presents the results of a study on the thermal conductivity of a nanoreinforced laminated composite (NRLC) comprising a carbon nanotube (CNT) array polymeric nanocomposite layer that is interspersed between the interfaces of the composite laminae. This NRLC is known to exhibit higher interlaminar shear properties than laminated composite materials without the array. The in-plane and through-the-thickness thermal conductivities of the NRLC and the corresponding laminated composite without the array were measured and compared to determine the effect of the array. In addition, a unit cell model was used to determine the thermal conductivity of the nanocomposite layer. It was observed that the array increases the thermal conductivity in the in-plane directions and does not significantly affect it in the through-the-thickness direction of the laminated composite.

KEY WORDS: nanocomposite, laminate, carbon nanotube, interphase, thermal conductivity.

INTRODUCTION

HEAT TRANSPORT IN carbon fiber reinforced polymer composite materials is good in the fiber direction, but poor in the transverse direction to the fiber. This is due to the

*Author to whom correspondence should be addressed. E-mail: jlabot@gmail.com
Figures 1–4 appear in color online: http://jcm.sagepub.com

0021-9983/11/03 0321–20 $10.00/0 DOI: 10.1177/0021998310373512

relatively high axial thermal conductivity of the carbon fibers and the relatively low thermal conductivity of the polymeric matrix. Usually, carbon fibers are arranged in a two-dimensional, unidirectional, noncrimp, weave, or braid reinforcement. This arrangement leads to a much higher thermal conductivity in the plane of the laminate. There are thus two approaches to develop laminated composite materials with superior thermal conductivity in the transverse direction to the laminate: (1) arrange a higher percentage of carbon fibers in the transverse direction to the laminate; or (2) increase the thermal conductivity of the matrix. The former approach leads not only to a more isotropic thermal response of laminated composites as shown in recent studies [1,2] but also to a lower fiber volume fraction in the in-plane directions that in turn reduces the in-plane mechanical properties. The alternative approach is to substitute the matrix by a polymer nanocomposite matrix that provides a higher thermal conductivity in the transverse direction to the laminate. Nanocomposites [3–6] are usually formed by dispersing nanoparticles, such as platelets like clay [7–9], carbon nanotubes (CNTs) [10–12], fibers like nanofibers [13], particulates like silica [3,4], or expanded graphite [14], in a polymeric matrix. A significant improvement of the thermal properties of the polymer matrix can be achieved with metallic particles or carbon nanostructures like carbon black, expanded graphite, carbon nanofibers, or CNTs at concentrations in the range 1–5% in volume [3,15]. A CNT is an excellent nanofiller due to its high mechanical, electrical, and thermal properties [10,11] and may be used for increasing heat transport in the resulting nanocomposites.

An individual CNT, which may be thought of as a rolled-up structure of a graphene sheet, exhibits exceptional physical properties due to its carbon defect-free structure. Indeed, molecular dynamics simulation studies have predicted thermal conductivities ranging between 3000 and 6600 W/m/K for individual single-walled carbon nanotubes (SWCNTs) and multi-walled carbon nanotubes (MWCNTs) [16–18]. However, experimental determination of their thermal conductivity shows values ranging from 300 to 3500 W/m/K [19–23]. This wide variation in the reported values may be attributed to the inherent difficulty in measuring temperatures at very small scales as required by some experimental methods.

While individual nanotubes have superior axial thermal properties, the practical application of the nanotubes in composites necessitates their use in the form of bundles, which in effect reduces the efficacy of thermal transport as compared to an individual nanotube due to various factors. Among them are: (1) the presence of multiple junctions (and hence scattering centers) between the tubes; (2) the interface between a nanotube and the matrix in which it is embedded; (3) defects in the nanotubes that are introduced during their growth. In fact, it has been shown that the thermal conductivity can decrease to 35 W/m/K in the case of a SWCNT 'mat' formed by a tangled bundle [18]. This degradation in the thermal property can be mitigated by the utilization of aligned nanotubes in the form of an array. It has been shown that when CNTs are aligned, the thermal conductivity is increased in the direction of alignment and reduced in the perpendicular direction, thereby resulting in anisotropy [24]. This effect can be exploited by orienting the nanotubes in the direction of the preferred heat transport.

The thermal response of the nanotubes is governed by phonons rather than by electrons [17] and the outer walls of the CNTs contribute more than the inner walls to thermal transport [19]. It is also known that the acoustic phonon states are the ones that contribute the most to the thermal conductivity. It is thus expected that the longer the CNTs, the higher the number of defects, which enhances phonon scattering and reduces their thermal transport capability [25]. This would definitely be the case for centimeter-long

MWCNT arrays. In-plane heat transport mechanisms involve junctions formed between neighboring bundles, and heat follows a tortuous path along the bundles and across the junctions. The effect of incorporating CNTs on the thermal properties of the resulting nanocomposites is described in the next sections.

It has been shown that the thermal conductivity in nanocomposites varies with the concentration of CNTs, increasing by 60% over that of pure epoxy for 5% CNT concentration [26]. It has also been shown that the thermal conductivity increases even further, 87%, for 0.99% silane-modified MWCNT content in a polymethylmethacrylate (PMMA) matrix [27]. The increase in thermal conductivity with increasing CNT concentration is nearly linear, unlike electrical conductivity, where a sharp percolation threshold is observed [28,29]. It has also been shown that the thermal conductivity decreases for concentrations higher than 10% [30]. This may be attributed to the increase in physical interactions between the nanoparticles and to rheological constraints, which restrict the dispersion of the CNTs in the matrix resulting in the formation of agglomerates. The interfacial thermal resistance between the polymer matrix and the CNTs as well as their structure, defects, aggregation, twist, and degree of alignment affect the thermal conductivity of the nanocomposite. The nanotube/matrix interfacial thermal contact resistance can arise from poor mechanical or chemical adherence at the interface and result in reduction of thermal conductivity.

The thermal conductivity of the nanocomposites is strongly dependent on the direction, aspect ratio, and volume fraction of the MWCNT phase. Experimental results show that the thermal conductivity in the axial direction of MWCNTs varies between 0.13 and 0.3 W/m/K for aspect ratios of 0 and 1200, respectively, and it increases by about 280%, from 0.16 to 0.61 W/m/K, for a volume fraction increase from 0.1 to 0.6 [31]. For this same range, it increases by more than 115%, from 0.13 to 0.28 W/m/K, in the transverse direction, and by less than 1% for a randomly oriented phase (about 0.12 W/m/K) [31]. Experimentally measured values confirm numerical results based on the asymptotic expansion homogenization (AEH) technique [32,33]. In nanocomposites with a randomly dispersed nanotube loading, long nanotubes are mostly not aligned and the concept of length efficiency could be considered in a theoretical model to predict the thermal conductivity of the composite. Modeling results have shown that length efficiency plays a fundamental role in the thermal conductivity of these nanocomposites, and thus the interfacial thermal resistance plays a smaller role [34].

Recent studies indicate that a vertically aligned MWCNT array embedded in a composite can provide direct channels for transmitting heat and more effectively increase the thermal conductivity of the composite [35]. It is well known that uniform dispersion of the nanotube phase within the polymeric matrix and improved nanotube/matrix wetting and adhesion are critical issues in the processing of nanocomposites [5]. The thermal conductivity of the nanocomposite could be increased due to the enhanced wettability and the formation of a network structure within the polymeric matrix by surface modification of the CNT arrays.

Nanocomposites can also constitute the matrix of laminated composites and improve the matrix-dominated mechanical and thermal properties of the resulting hierarchical composites. The thermal conductivity of laminated composites can be calculated from the thermal conductivities of the composite phases, that is, fiber and matrix. Homogenization techniques including the rule of mixtures, parallel and series models, and other empirical methods can be used with the thermal/electrical analogy to predict the thermal conductivity of composites. A good agreement between experimental and

finite element results has been shown for a set of composite materials over a wide range of fiber volume fractions [36]. Potential sources for discrepancy between the predicted and experimental results could reside in the fact that the heat flow was assumed to be one-dimensional and the thermal resistance between the fiber and the matrix assumed to be zero. It has also been shown that the in-plane thermal conductivity varies linearly with the fiber volume fraction [37].

A laminated composite material with higher thermal conductivity and with more efficient heat dissipation in all directions is needed for high-performance applications. This article focuses on the conductive heat transport of the CNT array nanoreinforced laminated composite (NRLC) and that of the corresponding laminated composite without the array. Their thermal conductivities in all directions were determined experimentally and the effect of the array height was considered for the NRLC. The thermal conductivity of the array nanocomposite layer was derived and calculated from the previous experimental results.

NANOREINFORCED LAMINATED COMPOSITE

The NRLC constitutes a novel structural concept comprising a MWCNT array polymeric nanocomposite layer that is interspersed between the plies of a laminated composite consisting of a microscale fiber reinforcement and a polymeric matrix [38]. The NRLC exhibits higher interlaminar shear properties than laminated composites without the arrays and does not require dispersion of the nanotubes into the polymeric matrix, thus simplifying its processing and allowing high nanoparticle contents [38]. The MWCNT consists of an average structure of approximately 10 walls with an outer diameter of 15 nm and an inner diameter of 4–5 nm. In this study, the MWCNT array height can vary between 100 μm and 1 mm. A thermosetting polymer matrix, diglycidyl ether of bisphenol-A (DGEBA) epoxy, and a two-dimensional plain woven fabric reinforcement [39–41], constitute the other phases of the NRLC. A schematic illustration of the fabrication steps of the NRLC is shown in Figure 1 [38,42].

In fiber reinforced polymeric composites, the fiber–matrix interphase plays a fundamental role in the in-plane transverse to the fiber and interlaminar stiffnesses and strengths. The physical and mechanical properties of the interphase are unique and

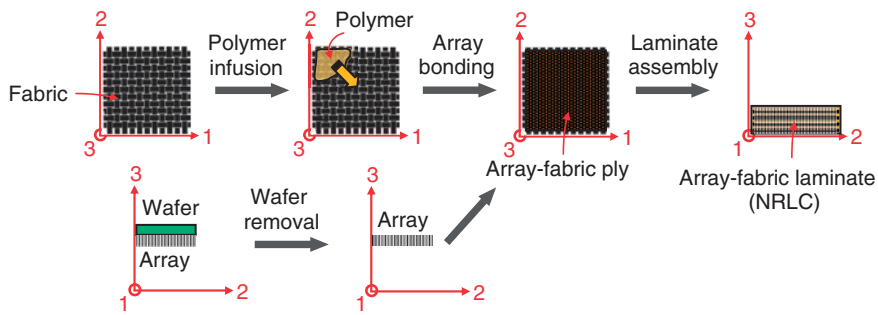

Figure 1. *Schematic illustration of fabrication steps of nanoreinforced laminated composite (NRLC) [38]. Note: '1' and '2' represent the direction of the carbon tows while '3' represents the transverse direction to the laminate and the initial direction of the MWCNT array.*

different from those of the fiber or the matrix [43–45]. The properties of the fiber–matrix interphase are not a decisive factor in determining the interlaminar fracture toughness in composites [41,43]. However, this is not the case in the NRLC because the pure matrix region is no longer present, creating thus a new interphase with the potential for exceptional bonding/interlocking capabilities.

An environmental scanning electron microscope (ESEM) image of the cross-section of a NRLC sample is shown in Figure 2. It shows the microscale reinforcement layers consisting of fiber tows aligned in the warp and fill directions (1- and 2-directions, respectively) and the MWCNT array polymeric nanocomposite layer. The initial array thickness decreases during the consolidation stage of the curing process of the composite. The NRLC fabrication process plays a crucial role in determining the interphase features, in particular, the final nanocomposite layer height. A study on the thermal conductivities of the NRLC and the laminated composite without the array is presented in the next section.

THERMAL CONDUCTIVITY

Formulation and Experimental Setup

The thermal conductivity of the composites was experimentally determined by a one-dimensional steady-state method similar to that of ASTM Standard D5470 [46].

The governing equation of the conductive heat transport or transfer is given by:

$$\operatorname{div} q = 0, \tag{1}$$

where q is the heat flux. The Fourier law is given by:

$$q = -k \cdot \operatorname{grad}(T), \tag{2}$$

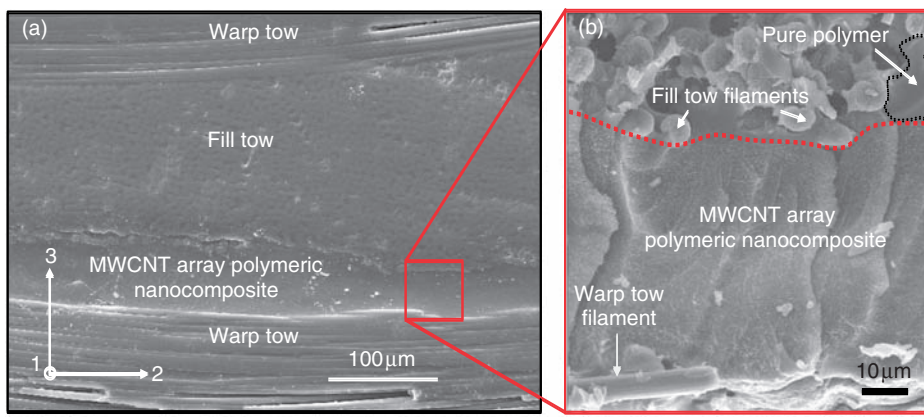

Figure 2. *ESEM images of the cross-section of NRLC and its phases: (a) MWCNT array polymeric nanocomposite layer bonded to the warp and fill tows; (b) closed-up image of nanocomposite layer [38]. Note: The phases are: 362 g/m^2 6k warp/fill Toray T300-40D carbon plain woven fabric; Toolfusion^R 1A-1B epoxy; and 500 μm-tall MWCNT array.*

where T is the temperature and k is the thermal conductivity. By applying Equation (2) to the composite sample shown in Figure 3 and integrating the flux over its constant cross-sectional area A, the equation of heat transport in the z- or 3-direction becomes:

$$Q = kA\frac{\mathrm{d}T}{\mathrm{d}z}, \tag{3}$$

where Q is the entering heat flow. The thermal conductivity can then be calculated by:

$$k = \frac{Qt}{A(T_\mathrm{u} - T_\mathrm{l})}, \tag{4}$$

where T_u is the upper surface temperature, T_l, the lower surface temperature, and t is the thickness of sample. The heat flow is measured directly by calculating the power that goes into a strain gage that serves as the heat source for the composite sample. The thermal gradient is determined by measuring the temperature with thermocouples placed at different locations throughout the composite sample. A similar experimental technique like the guarded heat flow method that could prevent radiation and convective heat losses was not used since these effects are negligible for the considered temperature range (less than 100°C). Measurements were done along the in-plane (1- or 2-) directions and out-of-plane (through-the-thickness, or transverse, or 3-) direction of the composite samples. Since a unidirectional heat flux is imposed, the only non-zero terms of the conductivity tensor lie in its diagonal and are the ones being calculated.

The power source that provides heat to the sample is an alternate current/direct current (AC/DC) adapter with a maximum current capacity of 500 mA. The input parameters of the adapter are: 120 V of alternating current; 12 W of power; and 60 Hz of frequency. The output parameter is 12 V of DC. A linear taper potentiometer is used to vary the incoming voltage from the power adapter. The potentiometer has a resistance of 1 MΩ with a tolerance of ±20% and the rated power is 0.5 W. A USB 6008 voltage data acquisition reader unit is used to monitor and record the voltage. The unit has eight analog channels with a resolution of 12 bits and an input impedance of 144 kΩ. The minimum voltage it can read is 1 V with an accuracy of 37.5 mV and the maximum voltage is 10 V with an accuracy of 138 mV. LabView SignalExpress™ 3.0 is used to record the voltage readings.

A strain gage is used as the heat source for the composite sample. The strain gage has a grid resistance of 120 Ω with a tolerance of ±0.5%. The current on the strain gage is measured using an ammeter. It has a 5½ digit resolution to measure DC voltage from 1 μV per count to 1000 V. It can measure currents from 1 nA to 10 A. The strain gage is

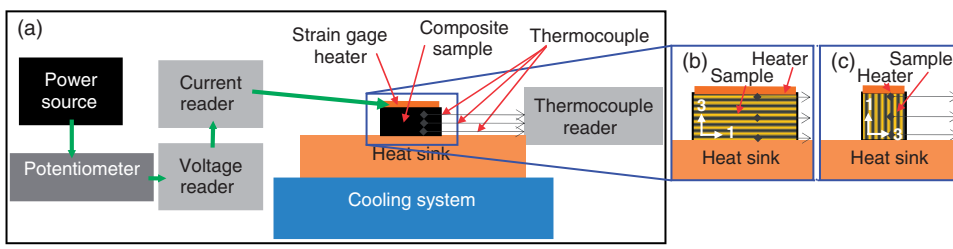

Figure 3. *(a) Schematic illustration of the experimental setup for thermal conductivity measurements; (b and c) schematic illustration of composite sample, heater, heat sink, and thermocouple configuration plus corresponding system of coordinates for through-the-thickness and in-plane direction measurements, respectively.*

bonded to the composite sample using an Arctic silver (Ag) paste adhesive with a thermal conductivity of about 8 W/m/K. To ensure steady state measurements, the composite sample is bonded to a copper block that is kept at a constant temperature. The bonding between them is similarly achieved using the Arctic Ag adhesive. The copper block is maintained at a constant temperature by placing it on a metal container that is cooled by circulating water in a 6000 cm^3 tank. This ensures that heat conduction takes place only in one direction.

In order to ensure zero stability in the strain gage, a maximum excitation voltage is recommended by its manufacturer depending on the type of gage and resistance. In the case of the EA125AD (120 Ω) gage for example, a maximum power density in the range of 0.31–0.78 mW/mm^2 is recommended for moderate measurement accuracy in a material with a thermal conductivity range like that of the composite samples. This power density corresponds to about 0.44–1.12 V for a current of 7 mA. Higher voltages would cause a drift due to the differential expansion of the strain gage constituent materials, Constantan alloy in the circuit and polyimide in the backing, which have dissimilar coefficients of thermal expansion.

The temperature is monitored with three temperature sensors (thermocouples) attached to the composite sample and one attached to the copper block. The thermocouples are a type K (Chromega®/Alomega®) unsheathed fine gage. The maximum service temperature of the thermocouples is 593°C and the response time for the 0.125 mm diameter wire in still air is 1.0 s. An epoxy adhesive, OB 101-2 from Omega, is used to bond the thermocouples to the sample. The thermal conductivity of the epoxy adhesive is 1.04 W/m/K and the electrical insulation bulk resistivity is 10^{15} Ω cm. The adhesive cures at room temperature and it is rated for continuous use until 105°C. The exact location of the thermocouples in the sample is determined using a microscope. A USB-TC reader is used to record the temperature readings. The reader has eight channel inputs with a 24-bit resolution. The differential input voltage range is ±0.080 V and the impedance is 5 GΩ. For a temperature range 0–1372°C, the maximum error is ±0.691°C, while the typical error is ±0.345°C. Tracer DAQ™ software is used to record the temperature and time and can export the results into an Excel™ file. The temperature and voltage can thus be recorded at every instant of time.

The strain gage is kept at a specific voltage by the voltage controller that is connected to the strain gage. Since the voltage is directly proportional to the temperature, a change in voltage would trigger a change in temperature. Therefore, the voltage is set to a constant value to enable recording steady state temperature measurements. A DC voltage output from the adapter is kept constant by using the potentiometer. One set of wires from the potentiometer is connected to the voltage reader, which in turn is connected to a port of the computer. The other set of wires provides the necessary power input to the strain gage. The voltage is set to a certain value and readings are recorded at every instant of time until it reaches a steady state value. The sample is then allowed to cool to room temperature. The time taken to reach the initial temperature is also noted. Two more readings at the same voltage are recorded. This is done to check the repeatability and accuracy of the measurements. Next, the voltage is set to another value and a similar procedure is followed. Measurements are taken for three different voltage values.

The experimental factors that affect the thermal conductivity measurements include loss due to convection and radiation, and random and systematic errors due to a variety of factors. In order to minimize convection and radiation losses, the experiments are performed in still air, and the samples are enclosed in a cup and covered with rubber pads on

their sides. The convection loss is minimal. The radiative heat loss is much smaller than the convective heat loss and can thus be neglected. Random errors are caused by fluctuations in voltage and current. These errors are minimized by using an adapter and a potentiometer to regulate the power applied at the strain gage heater. Systematic errors are caused by human misinterpretations and can be minimized by taking repeated readings and averaging them out. In this experimental study, a source of systematic error is due to incorrect measurement of the thermocouple location using the microscope. There are other sources of error including: interface thermal resistance between the strain gage and the composite sample, and between the composite sample and the copper block; unaccountable causes in the manufacturing process and handling technique; typical error in the USB-TC ($\pm 0.345^{\circ}$C) or $\pm 0.8^{\circ}$C when the temperature is higher than 35°C; and error in the voltage reader of around 7.23 mV. The deviation of the thermal conductivity is calculated using Equation (3).

Experimental Results

The measured thermal conductivities at room temperature of the laminated composite (16-ply 6k Toray T300-40D carbon plain woven fabric with 11 tows per 25.4 mm in the warp and fill directions and Toolfusion epoxy matrix) with a volume fraction of 65% is given in Table 1. The measured thermal conductivities at room temperature of the NRLC with the same fiber, matrix, and MWCNT arrays of two different heights are presented in Table 2. The thermal conductivities are average values for samples containing many woven fabric cells. The total random and systematic error is estimated to be 3.91% for the laminated composite and NRLC samples.

Table 1. Measured thermal conductivities of the composite laminate.

Parameter	Value
Number of woven fabric layers, n	16
Thickness of laminate, h_{tot} (mm)	4.2
Thermal conductivity of laminate in fill direction, k_{fc} (W/m/K)	3.42
Thermal conductivity of laminate in warp direction, k_{wc} (W/m/K)	3.42*
Thermal conductivity of laminate in transverse direction, k_{tc} (W/m/K)	0.77

*Estimate based on the fact that the woven fabric is balanced (same tow density in the warp and fill directions).

Table 2. Measured thermal conductivities of the NRLC.

Parameter	Value	Value
Number of woven fabric layers, n	3	7
Number of nanocomposite layers, n_{nano}	2	6
Thickness of MWCNT array before consolidation, h_{array} (μm)	100	500
Thickness of laminate, h_{tot} (mm)	0.733	1.750
Thermal conductivity of laminate in fill direction, k_{fc} (W/m/K)	10.40	13.97
Thermal conductivity of laminate in warp direction, k_{wc} (W/m/K)	10.40*	13.97*
Thermal conductivity of laminate in transverse direction, k_{tc} (W/m/K)	1.1	1.18

*Estimate based on the fact that the woven fabric reinforcement is balanced.

The thermal conductivity values of the composite laminate are similar to those previously measured of similar carbon/epoxy plain woven fabric laminated composites [47–49]. It is observed from Table 1 that the thermal anisotropy ratio between the in-plane and transverse thermal conductivities is approximately 4.44 (fiber volume fraction of 65%), which is similar to those previously determined for similar composite materials: approximately 4 (fiber volume fraction of 49%) [47] and 4.8 (fiber volume fraction of 55–62%), respectively [49].

The NRLC samples have a MWCNT volume fraction between 18% and 22% and the MWCNT array height in Table 2 corresponds to the initial value before fabrication of the NRLC sample. During fabrication, that height is reduced due to the consolidation pressure and the alignment of the nanotubes in the resulting nanocomposite layer is significantly affected. Comparing the thermal conductivities of the laminate and the NRLC from Tables 1 and 2, it is observed that the thermal conductivity of the NRLC increases in the transverse direction (between 43% and 53% depending on the MWCNT array height) and significantly increases in the in-plane directions (between 204% and 308% depending on the MWCNT array height). These changes are attributed to the presence of a high percentage of nanotubes that are originally aligned in the through-the-thickness direction but become aligned in the warp or fill directions during the consolidation stage. The increase of the thermal conductivity in the transverse direction can be attributed to the fraction of nanotubes that remain aligned in the through-the-thickness direction. The modeling effort to determine the thermal conductivity of the nanocomposite layer is presented in the next section.

Model Formulation

The thermal–electrical analogy is the most common method used to compute the thermal conductivity of woven fabric laminated composite materials [36,37,50,51]. This analogy is established based upon the similarity between the partial differential equations that govern the thermal potential (temperature), T, and the electrical potential (electromotive force), E, fields [37,50]. By using this analogy, the woven fabric laminated composite is transformed into an electrical circuit where the resistance can then be computed. The circuit model is characterized by the selection of a unit cell, which encloses the smallest periodic repeated volume in the laminate [36]. The material is considered to be homogeneous, and this assumption could certainly bring errors in the model due to resin-rich areas and nesting in the woven fabric composites [49].

COMPOSITE PHASES

The thermal conductivities of the composite phases that need to be defined are the conductivities in the axial and transverse directions of the fiber (k_{fa} and k_{ft}, respectively) and that of the isotropic matrix (k_m).

TOWS

Once the tow volume fraction is known, the thermal conductivity of the tows in the axial and transverse directions can be predicted by various models, including the series and parallel models, or by empirical methods. Knowing the properties of the fibers, the tow's axial thermal conductivity, k_{ta}, can be calculated from the rule of mixtures or

parallel model:

$$k_{ta} = v_{ft}k_{fa} + (1 - v_{ft})k_m. \tag{5}$$

The tow's transverse thermal conductivity, k_{tt}, can be calculated by the series model:

$$\frac{1}{k_{tt}} = \frac{v_{ft}}{k_{ft}} + \frac{(1 - v_{ft})}{k_m}, \tag{6}$$

or by the semi-empirical Clayton model [52]:

$$k_{tt} = k_m \left[\frac{\sqrt{(1 - v_{ft})^2 \left(\frac{k_{ft}}{k_m} - 1\right)^2 + 4k_{ft}/k_m} - (1 - v_{ft})\left(\frac{k_{ft}}{k_m} - 1\right)}{2} \right]^2, \tag{7}$$

or by the Pilling model [53]:

$$k_{tt} = k_m \frac{(1 - v_{ft}) + (1 + v_{ft})(k_{ft}/k_m)}{(1 - v_{ft})(k_{ft}/k_m) + (1 + v_{ft})}, \tag{8}$$

where v_{ft} is the fiber volume fraction of the tow.

The thermal conductivity of the tow in a direction forming an angle $\overline{\theta_i}$ with the axial direction can be calculated by the transformation:

$$k_i = k_{ta} \sin^2\overline{\theta_i} + k_{tt} \cos^2\overline{\theta_i}, \tag{9}$$

where $i = 1, 2$.

LAMINA

A composite lamina is a periodic material, and therefore, a representative volume element (RVE) can be considered in a model to predict its properties (Figure 4). The model is characterized by the selection of a unit cell, which encloses the smallest periodic repeated

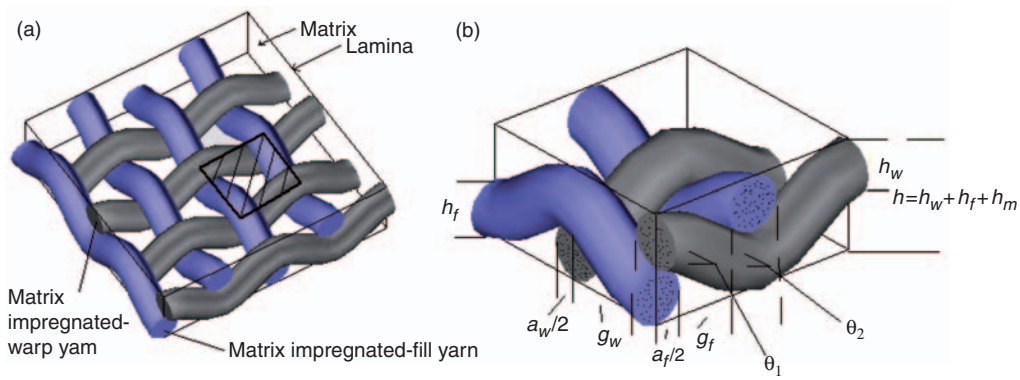

Figure 4. *(a) Idealized unit cell of the plain-woven fabric composite lamina; (b) RVE of plain woven fabric [36].*

volume in the laminate [36]. The lamina properties can now be calculated from the tow properties.

Assuming a balanced reinforcement (same tow density in the warp and fill directions), the transverse or through-the-thickness effective thermal conductivity of the lamina, k_t, is given by [36]:

$$k_t = \frac{k_m}{\left(1+\frac{g}{a}\right)^2}\left[\begin{array}{l}\dfrac{1}{\dfrac{h_m}{h}+\left(1-\dfrac{h_m}{h}\right)\dfrac{k_m}{k_2}}+\alpha\dfrac{g/a}{\left(1+\dfrac{h_m}{h}\right)+\left(1-\dfrac{h_m}{h}\right)\dfrac{k_m}{k_2}} \\ \quad +\beta\dfrac{g/a}{\left(1+\dfrac{h_m}{h}\right)+\left(1-\dfrac{h_m}{h}\right)\dfrac{k_m}{k_1}}+\left(\dfrac{g}{a}\right)^2\end{array}\right], \tag{10}$$

where

$$\alpha = \frac{132c_1 + 28c_2 + 20c_3 + 12c_4}{39c_1 + 9c_2 + 7c_3 + 8c_4 + 1}, \tag{11}$$

and

$$\beta = \frac{24c_1 + 8c_2 + 8c_3 + 12c_4 + 4}{39c_1 + 9c_2 + 7c_3 + 8c_4 + 1}, \tag{12}$$

where k_1 and k_2 are the thermal conductivities of the tow with the respective mean fiber inclination angles $\bar{\theta}_1$ and $\bar{\theta}_2$; g is the tow gap between two neighboring tows; a is the tow width between two neighboring tows; h_m is the thickness of the matrix layer; h is the thickness of the lamina; and α and β are geometrical parameters that depend on c_i, which are introduced to facilitate the analysis of various woven fabrics [36]. In the case of a plain woven fabric, for example, $c_i = 0$, and thus $\alpha = 0$ and $\beta = 4$.

The in-plane effective thermal conductivity of the lamina in the warp direction, k_w, is given by [37]:

$$k_w = \frac{1+\dfrac{g_f}{a_f}}{1+\dfrac{g_w}{a_w}}\left\{\begin{array}{l}\dfrac{k_m}{1+\dfrac{g_f}{a_f}}\left[\left(1+\dfrac{g_w}{a_w}\right)\dfrac{h_m}{h}+\dfrac{g_w}{a_w}\dfrac{h_w}{h}\right]+\dfrac{h_f}{h}\dfrac{g_w}{a_w}\left(\dfrac{1}{k_{f1}}+\dfrac{g_f}{a_f}\dfrac{1}{k_m}\right)^{-1} \\ \quad +\dfrac{h_f}{h}\dfrac{1}{\dfrac{1}{k_{f2}}+\dfrac{g_f}{a_f}\left[\dfrac{1}{2}k_m+\left(\dfrac{1}{k_m}+\dfrac{1}{k_{w1}}\right)^{-1}\right]^{-1}} \\ \quad +\dfrac{1}{k_{w2}\dfrac{h_w}{h}+\dfrac{g_f}{a_f}\left[k_{w1}\left(\dfrac{h_w}{h}-\dfrac{1}{2}\dfrac{h_f}{h}\right)+\dfrac{h_f}{h}\left(\dfrac{1}{k_{w1}}+\dfrac{1}{k_m}\right)^{-1}\right]^{-1}}\end{array}\right\}, \tag{13}$$

where k_{wi} and k_{fi} are the thermal conductivities of the impregnated tows taking into account the mean fiber inclination angle, which are computed from:

$$k_{wi} = k_{ta}\cos^2\bar{\theta}_i + k_{tt}\sin^2\bar{\theta}_i \ (i = 1, 2), \tag{14}$$

and

$$k_{fi} = k_{tt} \ (i = 1, 2). \tag{15}$$

The in-plane effective thermal conductivity of the lamina in the fill direction, k_f, is given by inverting the subscripts f and w in Equation (13):

$$k_f = \frac{1+\frac{g_w}{a_w}}{1+\frac{g_f}{a_f}} \left\{ \begin{array}{l} \dfrac{k_m}{1+\frac{g_w}{a_w}} \left[\left(1+\frac{g_f}{a_f}\right)\frac{h_m}{h} + \frac{g_f}{a_f}\frac{h_f}{h} \right] + \frac{h_w}{h}\frac{g_f}{a_f}\left(\frac{1}{k_{w1}} + \frac{g_w}{a_w}\frac{1}{k_m}\right)^{-1} \\ \quad + \dfrac{h_w}{h} \dfrac{1}{\frac{1}{k_{w2}} + \frac{g_w}{a_w}\left[\frac{1}{2}k_m + \left(\frac{1}{k_m} + \frac{1}{k_{f1}}\right)^{-1}\right]^{-1}} \\ \quad + \dfrac{1}{k_{f2}\frac{h_f}{h} + \frac{g_w}{a_w}\left[k_{f1}\left(\frac{h_f}{h} - \frac{1}{2}\frac{h_w}{h}\right) + \frac{h_w}{h}\left(\frac{1}{k_{f1}} + \frac{1}{k_m}\right)^{-1}\right]^{-1}} \end{array} \right\}. \tag{16}$$

The fiber volume fraction of the lamina, v_f, is calculated by [36]:

$$v_f = v_{ft} \frac{\left(1 - \frac{h_m}{h}\right)}{\left(1 + \frac{g_w}{a_w}\right)}. \tag{17}$$

COMPOSITE LAMINATE

An equivalent thermal circuit will be used to determine the properties of the composite laminate using the properties of each lamina. The composite laminate is to be formed with laminae consisting of a woven fabric reinforcement and a matrix material. The thermal conductivity of the composite laminate in the transverse direction can be determined by calculating the total resistance of the analog circuit (Figure 5) [50,51].

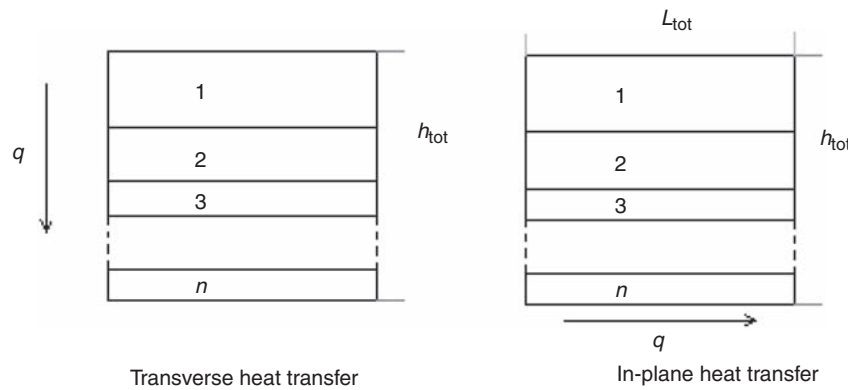

Figure 5. *Schematic illustration of the heat flow in a composite laminate composed of several laminae.*

The total resistance can be calculated by:

$$R_{\text{tot}} = \frac{h_{\text{tot}}}{k_{tc}A_{\text{tot}}} = \frac{h_1}{k_{t1}A_1} + \frac{h_2}{k_{t2}A_2} + \frac{h_3}{k_{t3}A_3} + \cdots + \frac{h_n}{k_{tn}A_n}, \tag{18}$$

where k_{tc} is the transverse thermal conductivity of the laminate, h_{tot} and A_{tot} are the total height and area, respectively, k_{tj} is the transverse thermal conductivity of each lamina, h_j is the thickness of each lamina, and A_j is the cross-sectional area perpendicular to the heat flow of each lamina. The cross-sectional area is the same for every lamina, and thus the transverse thermal conductivity for the composite laminate is given by:

$$k_{tc} = \frac{h_{\text{tot}}}{\sum_{j=1}^{n} \frac{h_j}{k_{tj}}}. \tag{19}$$

If the laminae are identical, the transverse thermal conductivity of the laminate will be equal to the thermal conductivity of the lamina.

Considering the same analogy to determine the thermal conductivity of the laminate in the warp direction, the resistance of the composite laminate can be calculated by:

$$\frac{1}{R_{\text{tot}}} = \frac{1}{\frac{L_{\text{tot}}}{k_{wc}A_{\text{tot}}}} = \frac{1}{\frac{L_1}{k_{w1}A_1}} + \frac{1}{\frac{L_2}{k_{w2}A_2}} + \frac{1}{\frac{L_3}{k_{w3}A_3}} + \cdots + \frac{1}{\frac{L_n}{k_{wn}A_n}}, \tag{20}$$

where k_{wc} is the thermal conductivity of the laminate in the warp direction, L_{tot} is the total length of the laminate, k_{wj} is the thermal conductivity in the warp direction of each lamina, L_j is the length of each lamina, and A_j is the cross-sectional area perpendicular to the heat flow of each lamina. In this case, the cross-sectional area will vary for each lamina. However, the length of each lamina will be identical to the length of the laminate. Thus:

$$k_{wc}A_{\text{tot}} = k_{w1}A_1 + k_{w2}A_2 + k_{w3}A_3 + \cdots + k_{wn}A_n. \tag{21}$$

This expression can be simplified even further by noticing that the area is the product of the thickness by the width. However, the width of each lamina is the same. Therefore, the thermal conductivity of the composite laminate in the warp direction can be computed by:

$$k_{wc} = \sum_{j=1}^{n} \left(\frac{k_{wj}h_j}{h_{\text{tot}}} \right). \tag{22}$$

The thermal conductivity of the laminate in the fill direction can be calculated in a similar manner.

Model Results

The thermal conductivities of the fiber and the matrix at room temperature are given in Table 3. The geometrical parameters of the 6k warp/fill Toray T300-40D (11 tows per 25.4 mm in the warp and fill directions) carbon plain-woven fabric are given in Table 4. The geometrical parameters and predicted thermal conductivities of the tow, lamina, and laminate are given in Tables 5–7, respectively. The values of the geometrical parameters were determined from optical micrographs, and the fiber volume fraction of the tow was

Table 3. Thermal conductivities of fiber and matrix [36].

Parameter	Value
Thermal conductivity of fiber in axial direction, k_{fa} (W/m/K)	8.40
Thermal conductivity of fiber in transverse direction, k_{ft} (W/m/K)	0.84
Thermal conductivity of matrix, k_m (W/m/K)	0.19

Table 4. Geometrical parameters of 6k warp/fill Toray T300-40D plain woven fabric.

Fabric parameter	Value
Gap between 2 tows in fill direction, g_f (m)	0.000145
Gap between 2 tows in warp direction, g_w (m)	0.000404
Width of fill tow, a_f (m)	0.001978
Width of warp tow, a_w (m)	0.001748
Thickness of matrix, h_m (m)	0.000080
Thickness of fill tow, h_f (m)	0.000244
Thickness of warp tow, h_w (m)	0.000244
Thickness of lamina, h (m)	0.000568
Mean inclination angle of g_f, g_w, $\bar{\theta}_1$ (rad)	0.29380
Mean inclination angle of other, $\bar{\theta}_2$ (rad)	0.103823

Table 5. Tow fiber volume fraction and predicted thermal conductivities of tow.

Parameter	Value
Fiber volume fraction of tow, v_{ft}	0.92
Thermal conductivity of tow in axial direction, k_{ta} (W/m/K)	7.743
Thermal conductivity of tow in transverse direction, k_{tt} (W/m/K)*	0.738

*Calculated by Clayton's model.

Table 6. Predicted thermal conductivities and geometrical parameters of plain woven fabric composite lamina.

Parameter	Value
k_1 (W/m/K)	1.325
k_2 (W/m/K)	0.813
k_{w1} (W/m/K)	7.156
k_{w2} (W/m/K)	7.668
$k_{f1} = k_{f2}$ (W/m/K)	0.738
α	0
β	4
Fiber volume fraction, v_f (%)	64.0
Thermal conductivity of lamina in fill direction, k_f (W/m/K)	2.841
Thermal conductivity of lamina in warp direction, k_w (W/m/K)	2.821
Thermal conductivity of lamina in transverse direction, k_t (W/m/K)	0.522

Table 7. Predicted thermal conductivities of plain woven fabric composite laminate.

Parameter	Value
Thermal conductivity of laminate in fill direction, k_{fc} (W/m/K)	2.841
Thermal conductivity of laminate in warp direction, k_{wc} (W/m/K)	2.821
Thermal conductivity of laminate in transverse direction, k_{tc} (W/m/K)	0.522

determined so that the fiber volume fraction of the composite lamina matched the experimentally measured value.

The standard deviations for the gap between the 2 tows in the warp direction, g_w, and the mean inclination angle of the gaps, $\bar{\theta}_1$, are 18% and 10%, respectively. The other parameters in Table 4 exhibit a standard deviation of less than 5%. These deviations will affect the prediction of the thermal conductivity of the composite lamina in all directions by at most 3%.

If the thermal conductivity of the tow in the transverse direction, k_{tt}, was calculated through the series model instead of the Clayton's model, the predicted in-plane and transverse thermal conductivities of the composite lamina would vary by 1% and 5.4%, respectively. Using the Pilling's model, those predicted thermal conductivities would vary by 0.3% and 1.5%, respectively.

The predicted values for the composite lamina and laminate in Tables 6 and 7 correspond to a fiber volume fraction of approximately 64% in the composite. The predicted values in Table 7 can be compared with the measured values in Table 1. The values differ by 17% and 32% for the in-plane and through-the-thickness thermal conductivities, respectively. These differences are attributed to the inability of the model to capture the thermal response of the composite sample, mainly in the through-the-thickness direction. Previous studies on unidirectional composites have addressed the difficulty in predicting their thermal conductivity when there is a significant difference in the values of the thermal conductivity of the composite phases [54]. In the case of composites with woven fabric reinforcements, previous studies found differences of up to 15% between experimental and predicted thermal conductivity values [49,55]. The model that was considered here [36] and similar ones [32] are based on a unit cell that does not consider nesting [49]. Studies with more detailed models like the Fabric Geometry Model [56] that do not consider a unit cell but the temperature-dependent thermal conductivity of the composite phases and the variation of the temperature field throughout the composite instead, determined differences of about 5% and 12% for the in-plane and transverse thermal conductivities, respectively [55]. Among the effects that may also play a role in the difference between the experimental and predicted thermal conductivities in this study are pores or cracks, local effects at fiber cross-overs, fibers that are twisted and not parallel in the tows, and the presence of an interfacial resistance between the fiber and the matrix [49,57,58].

The NRLC includes CNT array polymeric nanocomposite layers and their thermal conductivity cannot be measured independently since their configuration would be different outside the composite laminate. The thermal conductivity of this nanocomposite layer can, however, be calculated using the previous model and the experimental measurements.

Thermal Conductivity of Nanocomposite Layer

Rearranging Equation (19):

$$k_{tc} = \frac{h_{\text{tot}} k_t k_{t\text{nano}}}{n_{\text{nano}} h_{\text{nano}} k_t + nhk_{t\text{nano}}}, \tag{23}$$

where $k_{t\text{nano}}$ is the thermal conductivity of the nanocomposite layer in the transverse direction. It is thus given by:

$$k_{t\text{nano}} = \frac{n_{\text{nano}} h_{\text{nano}} k_t k_{tc}}{h_{\text{tot}} k_t - nhk_{tc}}. \tag{24}$$

For the thermal conductivity in the warp and fill directions, rearranging Equation (22):

$$k_{wc} = \frac{nhk_w + n_{\text{nano}} h_{\text{nano}} k_{w\text{nano}}}{h_{\text{tot}}}. \tag{25}$$

Thus, the thermal conductivity of the nanocomposite layer in the warp direction is:

$$k_{w\text{nano}} = \frac{h_{\text{tot}} k_{wc} - nhk_w}{n_{\text{nano}} h_{\text{nano}}}. \tag{26}$$

The predicted thermal conductivities of the nanocomposite layer for the different NRLCs are given in Table 8.

An accurate value of the nanocomposite layer thickness after consolidation is critical to be able to calculate its thermal conductivity values. However, this thickness varies significantly throughout the sample and its value can only be estimated from ESEM images. A set of minimum and maximum thickness values were considered (line 4 in Table 8) to determine the lower and upper bounds of the thermal conductivity values of the nanocomposite layer (lines 6–8 of Table 8). From the values of Table 8, it is observed that the transverse thermal conductivity of the nanocomposite layer is 10–18% higher than that of the carbon fabric composite lamina itself depending on the array thickness. In the warp or fill directions, however, the thermal conductivity of the nanocomposite layer is predicted to be in the approximate range of 202–344 W/m/K, or two orders of magnitude higher than that of the composite laminate without the nanocomposite layer. These thermal conductivity values are very high and cannot be confirmed by experiments at this time.

Table 8. Predicted thermal conductivities of nanocomposite layer of NRLC.

Parameter	Value	Value
Number of layers of woven fabric, n	3	7
Number of nanocomposite layers, n_{nano}	2	6
Thickness of MWCNT array before consolidation, h_{array} (μm)	100	500
Thickness range of nanocomposite layer, h_{nano} (μm)	23–40	23–50
Thickness of laminate, h_{tot} (m)	0.733	1.750
Thermal conductivity of nanocomposite layer (fill direction), $k_{f\text{nano}}$ (W/m/K)	202–344	278–341
Thermal conductivity of nanocomposite layer (warp direction), $k_{w\text{nano}}$ (W/m/K)	202–344*	278–341*
Thermal conductivity of nanocomposite layer (tow direction), $k_{t\text{nano}}$ (W/m/K)	0.91	0.85

*Estimate based on the fact that the woven fabric is balanced.

Thermal conductivity measurements were conducted on the CNT arrays themselves, without the polymer, and reported elsewhere [59].

SUMMARY AND CONCLUSIONS

The conductive heat transport in a laminated composite reinforced with a CNT array nanocomposite layer and the corresponding laminated composite without the array was investigated with a combined experimental and analytical study. The in-plane and through-the-thickness or transverse thermal conductivities of the composites were determined experimentally. The thermal conductivity of the nanocomposite layer was derived from a model and calculated using the experimental results. It was determined that the nanocomposite layer slightly increases the thermal conductivity of the laminated composite in the transverse direction and significantly increases its thermal conductivity in the in-plane directions. This was attributed to the in-plane alignment of most nanotubes within the nanocomposite layer during the composite fabrication. The in-plane thermal conductivity of the nanocomposite layer was estimated to be two orders of magnitude higher than that of the laminated composite, thus making it ideal for heat transport in that direction. Further studies are needed on the functionalization of highly dense and aligned CNT arrays and their integration into laminated composites to potentially achieve at least one order of magnitude higher thermal conductivity in the transverse direction of the laminate.

ACKNOWLEDGMENTS

The authors thank Dr. Vesselin N. Shanov, Dr. Mark J. Schulz, and their students, Mr. Chaminda Jayasinghe and Ge Li, for providing helpful suggestions and fabricating the nanotube arrays for the experimental section of this study. The measurement of the thermal impedance of some of the composite and MWCNT array samples by Dr. Pani Varanasi and Dr. Evan Thomas at the University of Dayton Research Group is greatly appreciated.

REFERENCES

1. Schuster, J., Heider, D., Sharp, K. and Glowania, M. (2008). Thermal Conductivities of Three-dimensionally Woven Fabric Composites, *Composites Science and Technology*, **68**(9): 2085–2091.
2. Sharp, K., Bogdanovich, A.E., Tang, W., Heider, D., Advani, S. and Glowiana, M. (2008). High Through-thickness Thermal Conductivity Composites Based on Three-dimensional Woven Fiber Architectures, *AIAA Journal*, **46**(11): 2944–2954.
3. Pinnavaia, T.J. and Beall, G.W. (2000). *Polymer–Clay Nanocomposites*, Wiley, Chichester, United Kingdom.
4. Friedrich, K., Fakirov, S. and Zhang, Z. (2005). *Polymer Composites: From Nano-to-Macro Scale*, Springer, New York.
5. Koo, J.H. (2006). *Polymer Nanocomposites: Processing, Characterization, and Applications*, McGraw-Hill, New York.
6. Thostenson, E.T., Li, C. and Chou, T.-W. (2005). Review: Nanocomposites in Context, *Composites Science and Technology*, **65**(3–4): 491–516.

7. Messersmith, P. and Giannelis, E.P. (1994). Synthesis and Characterization of Layered Silicate–Epoxy Nanocomposites, *Chemistry of Materials*, **6**(10): 1719–1725.
8. Abot, J.L., Yasmin, A. and Daniel, I.M. (2002). Mechanical and Thermoviscoelastic Properties of Clay/Epoxy Nanocomposites, In: *Materials Research Society Proceedings*, Boston, Massachusetts, USA, pp. 167–172.
9. Yasmin, A., Abot, J.L. and Daniel, I.M. (2003). Processing and Characterization of Clay/Epoxy Nanocomposites by Shear Mixing, *Scripta Materialia*, **49**(1): 81–86.
10. Iijima, S. (1991). Helical Microtubules of Graphitic Carbon, *Nature*, **354**(6348): 56–58.
11. Dresselhaus, M., Dresselhaus, G. and Avouris, P. (2002). *Carbon Nanotubes: Synthesis, Structure, Properties, and Applications*, Springer, New York.
12. Thostenson, E.T., Ren, Z. and Chou, T.-W. (2001). Advances in the Science and Technology of Carbon Nanotubes and their Composites, *Composites Science and Technology*, **61**(13): 1899–1912.
13. Klosterman, D., Williams, M., Heitkamp, C., Donaldson, R. and Browning, C. (2007). Fabrication and Evaluation of Epoxy Nanocomposites and Carbon/Epoxy Composite Laminates Containing Oxidized Carbon Nanofibers, *SAMPE Journal*, **43**(4): 7–17.
14. Yasmin, A., Luo, J.-J. and Daniel, I.M. (2006). Processing of Graphite Nanosheet Reinforced Polymer Nanocomposites, *Composites Science and Technology*, **66**(9): 1182–1189.
15. Evseeva, L.E. and Tanaeva, S.A. (2008). Thermal Conductivity of Micro and Nanostructural Epoxy Composites at Low Temperatures, *Mechanics of Composite Materials*, **44**(1): 87–92.
16. Berber, S., Kwon, Y.K. and Tomanek, D. (2000). Unusually High Thermal Conductivity of Carbon Nanotubes, *Physical Review Letters*, **84**(20): 4613–4616.
17. Che, J., Cagin, T. and Goddard, W.A. (2000). Thermal Conductivity of Carbon Nanotubes, *Nanotechnology*, **11**(2): 65–69.
18. Hone, J., Whitney, M., Piskoti, C. and Zettl, A. (1999). Thermal Conductivity of Single-walled Carbon Nanotubes, *Physical Review B*, **59**(4): R2514–R2516.
19. Kim, P., Shi, L., Majumdar, A. and McEuen, P. (2001). Thermal Transport Measurements of Individual Multiwalled Nanotubes, *Physical Review Letters*, **87**(21): 215502–215505.
20. Pop, E., Mann, D., Wang, Q., Goodson, K. and Dai, H. (2006). Thermal Conductance of an Individual Single-wall Carbon Nanotube above Room Temperature, *Nano Letters*, **6**(1): 96–100.
21. Fujii, M., Zhang, X., Xie, H., Ago, H., Takahashi, K., Ikuta, T., Abe, H. and Shimizu, T. (2005). Measuring the Thermal Conductivity of a Single Carbon Nanotube, *Physical Review Letters*, **95**: 0655021–0655024.
22. Choi, T.-Y., Poulikakos, D., Tharian, J. and Sennhauser, U. (2006). Measurement of the Thermal Conductivity of Individual Carbon Nanotubes by the Four-point Three-ω Method, *Nano Letters*, **6**(8): 1589–1593.
23. Choi, T.-Y., Poulikakosa, D., Tharian, J. and Sennhauser, U. (2005). Measurement of Thermal Conductivity of Individual Multiwalled Carbon Nanotubes by the 3-ω Method, *Applied Physics Letters*, **87**: 0131081–0131083.
24. Hone, J., Llaguno, M.C., Nemes, N.M., Johnson, A.T., Fischer, J.E., Walters, D.A., Casavant, M.J., Schmit, J. and Smalley, R.E. (2000). Electrical and Thermal Transport Properties of Magnetically Aligned Single Wall Carbon Nanotube Films, *Applied Physics Letters*, **77**(5): 666–668.
25. Xie, H.Q., Cai, A. and Wang, X.W. (2007). Thermal Diffusivity and Conductivity of Multiwalled Carbon Nanotube Arrays, *Physics Letters A*, **369**(1–2): 120–123.
26. Thostenson, E.T. and Chou, T.-W. (2006). Processing-structure-multi-functional Property Relationship in Carbon Nanotube/Epoxy Composites, *Carbon*, **44**(14): 3022–3029.
27. Yuen, S.-M., Ma, C.-C.M., Chiang, C.-L., Chang, J.-A., Huang, S.-W., Chen, S.-C., Chuang, C.-Y., Yang, C.-C. and Wei, M.-H. (2007). Silane-modified MWCNT/PMMA Composites – Preparation, Electrical Resistivity, Thermal Conductivity and Thermal Stability, *Composites Part A – Applied Science and Manufacturing*, **38**(12): 2527–2535.

28. Moisala, A., Li, Q., Kinloch, I.A. and Windle, A.H. (2006). Thermal and Electrical Conductivity of Single- and Multi-walled Carbon Nanotube–Epoxy Composites, *Composites Science and Technology*, **66**(10): 1285–1288.
29. Martin, C.A., Sandler, J.K.W., Shaffer, M.S.P., Schwarz, M.-K., Bauhofer, W., Schulte, K. and Windle, A.H. (2004). Formation of Percolating Networks in Multi-wall Carbon-nanotube–Epoxy Composites, *Composites Science and Technology*, **64**(15): 2309–2316.
30. Yuen, S.-M., Ma, C.C.M., Wu, H.-H., Kuan, H.-C., Chen, W.-J., Liao, S.-H., Hsu, C.-W. and Wu, H.-L. (2007). Preparation and Thermal, Electrical, and Morphological Properties of Multiwalled Carbon Nanotube and Epoxy Composites, *Journal of Applied Polymer Science*, **103**(2): 1272–1278.
31. Song, Y.S. and Youn, J.R. (2006). Evaluation of Effective Thermal Conductivity for Carbon Nanotube/Polymer Composites using Control Volume Finite Element Method, *Carbon*, **44**(4): 710–717.
32. Dasgupta, A., Agarwal, R.K. and Bhandarkar, S.M. (1996). Three-dimensional Modeling of Woven-fabric Composites for Effective Thermomechanical and Thermal Properties, *Composites Science and Technology*, **56**(3): 209–223.
33. Dasgupta, A. and Agarwal, R.K. (1992). Orthotropic Thermal Conductivity of Plain-weave Fabric Composites Using a Homogenization Technique, *Journal of Composite Materials*, **26**(18): 2736–2758.
34. Song, P.C., Liu, C.H. and Fan, S. (2006). Improving the Thermal Conductivity of Nanocomposites by Increasing the Length Efficiency of Loading Carbon Nanotubes, *Applied Physics Letters*, **88**(15): 153111–153113.
35. Huang, H., Liu, C., Wu, Y. and Fan, S. (2005). Aligned Carbon Nanotube Films for Thermal Management, *Advanced Materials*, **17**(13): 1652–1656.
36. Ning, Q.G. and Chou, T.-W. (1998). A General Analytical Model for Predicting the Transverse Effective Thermal Conductivities of Woven Fabric Composites, *Composites Part A – Applied Science and Manufacturing*, **29**(3): 315–322.
37. Ning, Q.G. and Chou, T.-W. (1995). Closed-form Solutions of the In-plane Effective Thermal Conductivities of Woven-fabric Composites, *Composites Science and Technology*, **55**(1): 41–48.
38. Abot, J.L., Song, Y., Schulz, M.J. and Shanov, V.N. (2008). Novel Carbon Nanotube Array-reinforced Laminated Composite Materials with Higher Interlaminar Elastic Properties, *Composites Science and Technology*, **68**(13): 2755–2760.
39. Chou, T.-W. (1992). *Microstructural Design of Fiber Composites*, Cambridge University Press, Cambridge.
40. Long, A.C. (2006). *Design and Manufacture of Textile Composites*, Woodhead, Cambridge.
41. Cox, B.N. and Flanagan, G. (1997). *Handbook of Analytical Methods for Textile Composites*, NASA Contractor Report 4750.
42. Abot, J.L., Schulz, M.J., Shanov, V., Song, Y., Gorton, A. and Yun, Y.-H. (2007). Delamination Resistant Carbon Nanotube Array Polymeric Composite Materials, Invention Disclosure UC 107-071, University of Cincinnati.
43. Kim, J.-K. and Mai, Y.-W. (1998). *Engineered Interfaces in Fiber Reinforced Composites*, Elsevier, Oxford.
44. Drzal, L.T., Rich, M.J. and Lloyd, P.F. (1982). Adhesion of Graphite Fibers to Epoxy Matrices. Part I. The Role of Fiber Surface Treatment, *Journal of Adhesion*, **16**(1): 1–30.
45. Drzal, L.T. and Madhukar, M. (1993). Fiber-matrix Adhesion and its Relationship to Composite Mechanical Properties, *Journal of Materials Science*, **28**(3): 569–610.
46. Parrot, J.E. and Stukes, A.D. (1975). *Thermal Conductivity of Solids*, Pion, London.
47. Sweeting, R.D. and Liu, X.L. (2004). Measurement of Thermal Conductivity for Fibre-reinforced Composites, *Composites Part A: Applied Science and Manufacturing*, **35**(7–9): 933–938.
48. Hind, S. and Robitaille, F. (2008). Measurement and Modelling of In-plane and Transverse Thermal Conductivity in Tape Prepreg, Non-woven and Woven Textile Composites, In: *Recent Advances in Textile Composites, 9th International Conference on Textile Composites*, Newark, Delaware, USA, pp. 298–305.

49. Hind, S. and Robitaille, F. (2009). Measurement, Modeling, and Variability of Thermal Conductivity for Structural Polymer Composites, *Polymer Composites*, **31**(5): 847–857.
50. Kulkarni, M.R. and Brady, R.P. (1997). A Model of Global Thermal Conductivity in Laminated Composite Materials, *Composites Science and Technology*, **57**(3): 277–285.
51. Seo, B.H., Cho, Y.J., Youn, J.R., Chung, K., Kang, T.J. and Park, J.K. (2005). Model for Thermal Conductivities in Spun Yarn Carbon Fabric Composites, *Polymer Composites*, **26**(6): 791–798.
52. Clayton, W.A. (1971). Constituent and Composite Thermal Conductivities of Phenolic-carbon and Phenolic-graphite Ablators, In: *12th Structures, Structural Dynamics, and Materials Conference Proceedings*, 19–21 April, AIAA, Anaheim, California, USA, pp. 71–380.
53. Pilling, M.W., Yates, B., Black, M.A. and Tattersall, P. (1979). Thermal-conductivity of Carbon Fiber-reinforced Composites, *Journal of Materials Science*, **14**(6): 1326–1338.
54. Wetherhold, R.C. and Wang, J.Z. (1994). Difficulties in the Theories for Predicting Transverse Thermal-conductivity of Continuous Fiber Composites, *Journal of Composite Materials*, **28**(15): 1491–1498.
55. Bigaud, D., Goyhénèche, J.-M. and Hamelin, P. (2001). A Global-local Non-linear Modelling of Effective Thermal Conductivity Tensor of Textile-reinforced Composites, *Composites Part A: Applied Science and Manufacturing*, **32**(10): 1443–1453.
56. Gowayed, Y. and Hwang, J.C. (1995). Thermal-conductivity of Composite-materials Made from Plain Weaves and 3-D Weaves, *Composites Engineering*, **5**(9): 1177–1186.
57. Mottram, J.T. and Taylor, R. (1987). Thermal Conductivity of Fibre-phenolic Resin Composites. Part I: Thermal Diffusivity Measurements, *Composites Science and Technology*, **29**(3): 189–210.
58. Mottram, J.T. and Taylor, R. (1987). Thermal Conductivity of Fibre-phenolic Resin Composites. Part II: Numerical Analysis, *Composites Science and Technology*, **29**(3): 211–232.
59. Abot, J.L., Raghavan, V., Li, G. and Thomas, E.L. Effect of Interface, Height and Density of Tall Carbon Nanotube Arrays on their Thermal Conductivity: An Experimental Study, *Journal of Nanoscience and Nanotechnology* (accepted).